Supporting Information for:

Differential lipid selectivity of StARD phospholipid transporters revealed by native MS

Carla Kirschbaum[a,b*], Sophie A. S. Lawrence[a,b], Jack L. Bennett[a,b], Olivia B. Ramsay[a,c], Yara Ahmed[d,e], Tarick J. El-Baba[a,b], Stefano Vanni[d,e], Carol V. Robinson[a,b*]

a Kavli Institute for Nanoscience Discovery, University of Oxford, Oxford OX1 3QU, United Kingdom

b Department of Chemistry, University of Oxford, Oxford OX1 3QZ, United Kingdom

c Department of Oncology, University of Oxford, Oxford OX3 7DQ, United Kingdom

d Department of Biology, University of Fribourg, Fribourg, Switzerland

e Swiss National Center for Competence in Research Bio-inspired Materials, University of Fribourg, Fribourg, Switzerland

Correspondence: carla.kirschbaum@chem.ox.ac.uk, carol.robinson@chem.ox.ac.uk

Contents

Overview of investigated proteins

Table S1. Expected and measured masses of proteins investigated in this work.

Protein	Expected mass (kDa)	Measured mass (KDa)
Expressed in *E. coli*		
STARD2	25.038	25.036
STARD2 R78Q	25.009	25.008
STARD7(76–370)	34.891	34.886
STARD7(76–370) R189Q	34.863	34.863
STARD10	33.242	33.238
STARD10 R92Q	33.215	33.214
Expressed in human cell lines		
STARD2-FLAG	28.333	28.375 (+42 Da)
STARD7-FLAG (79-370)	37.914	37.914
STARD10-FLAG	36.539	36.741 (+202 Da)

Characterization of StARD proteins expressed in *E. coli*

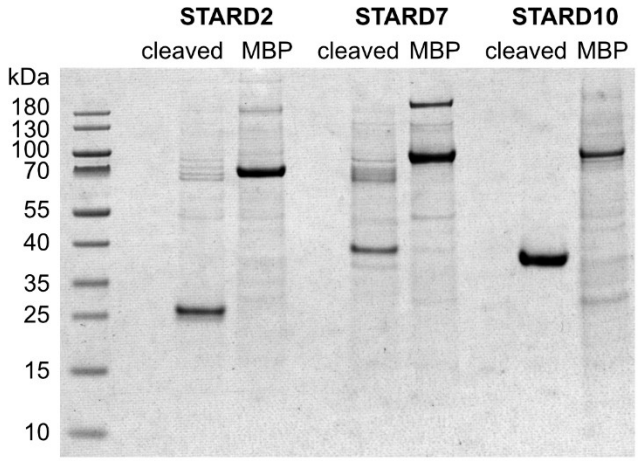

Figure S1. SDS-PAGE of STARD2, STARD7(76–370) and STARD10 expressed in *E. coli*, before and after cleavage of the N-terminal maltose-binding protein (MBP) tag.

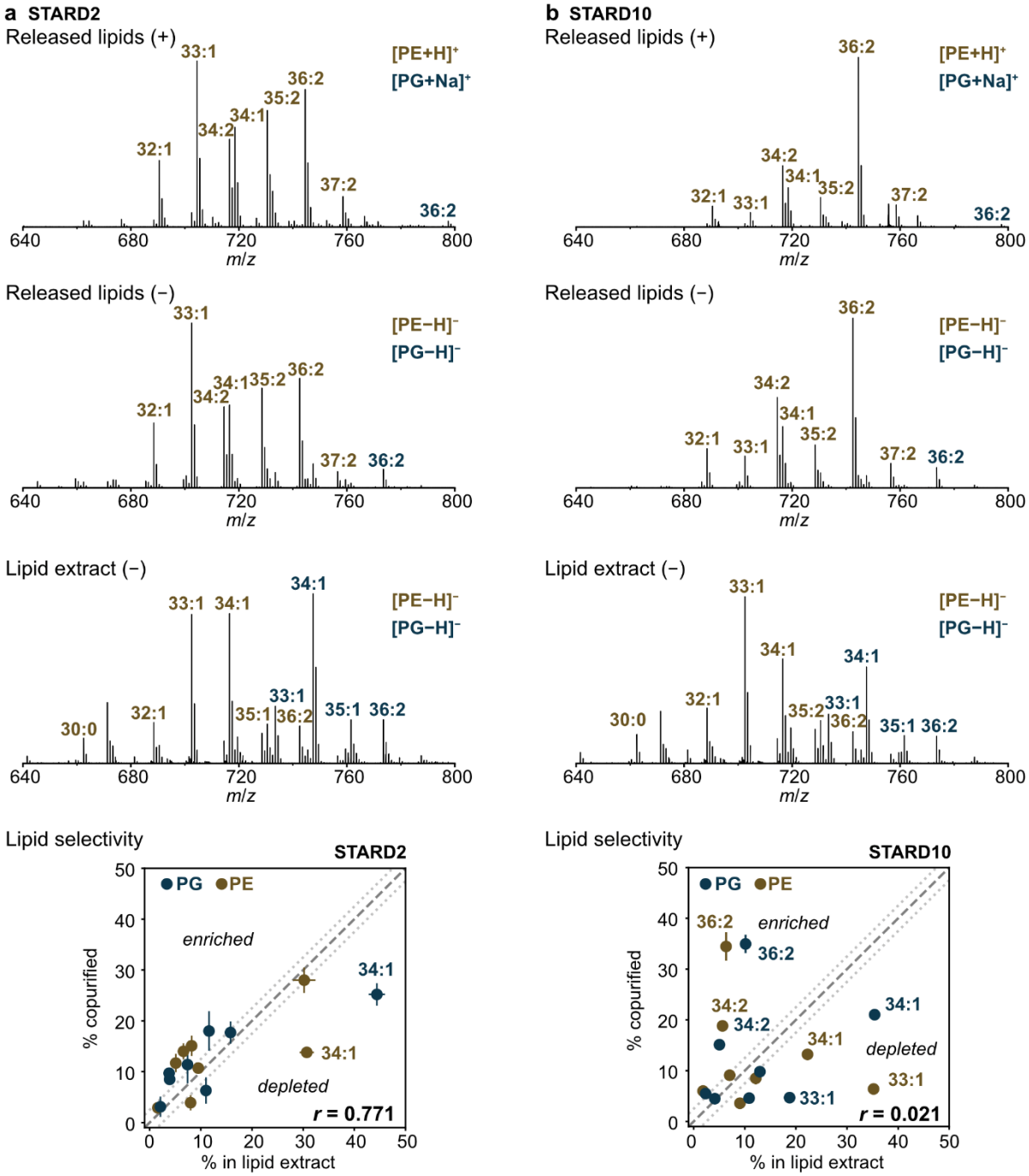

Figure S2. Lipids copurified with STARD2 and STARD10 upon expression in *E. coli*. **a.** PE and PG are released from STARD2 in positive and negative ion modes. The released lipids show a strong positive correlation with the bulk lipid composition of the STARD2-expressing cells (Pearson correlation coefficient = 0.771). **b.** PE and PG copurified with STARD10 show weak correlation with the membrane lipid composition of the STARD10-expressing cells (Pearson correlation coefficient = 0.021). PE and PG were quantified individually. The dotted grey lines indicate ±2.5% deviation from the diagonal. Error bars represent the standard deviation of triplicate measurements.

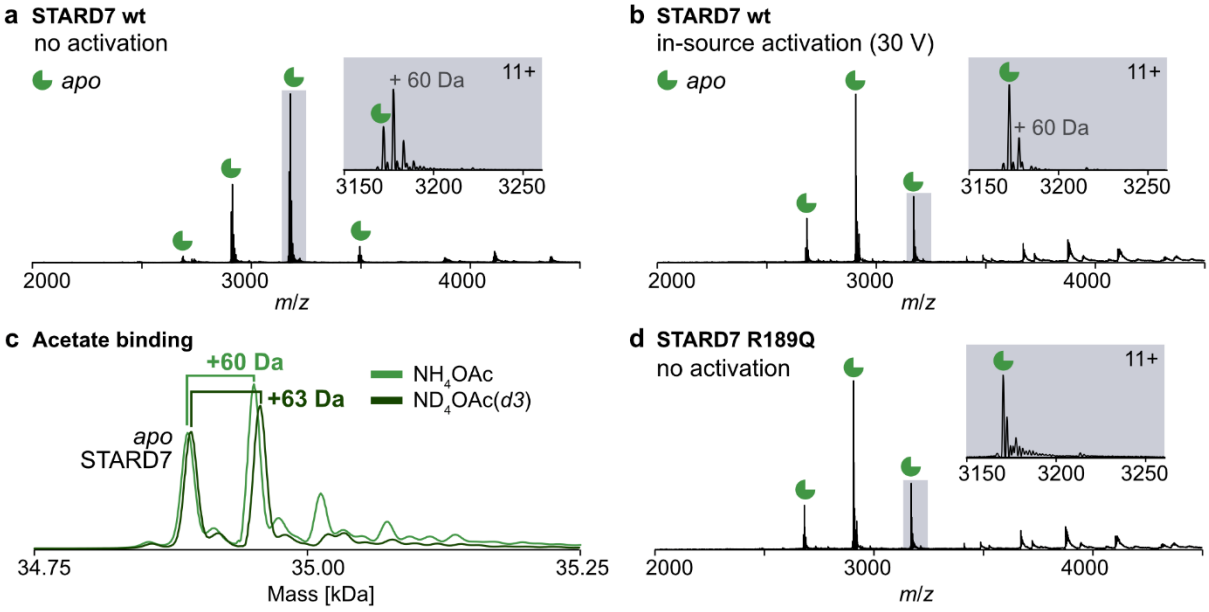

Figure S3. Acetate binding to STARD7. **a.** Wild-type STARD7(76–370) ionized in 200 mM ammonium acetate. **b.** Acetate dissociates from the protein with in-source activation (30 V). **c.** STARD7(76–370) ionized in 200 mM ammonium acetate-d7. **d.** The STARD7(76–370) R189Q mutant ionized in 200 mM ammonium acetate shows significantly reduced acetate binding.

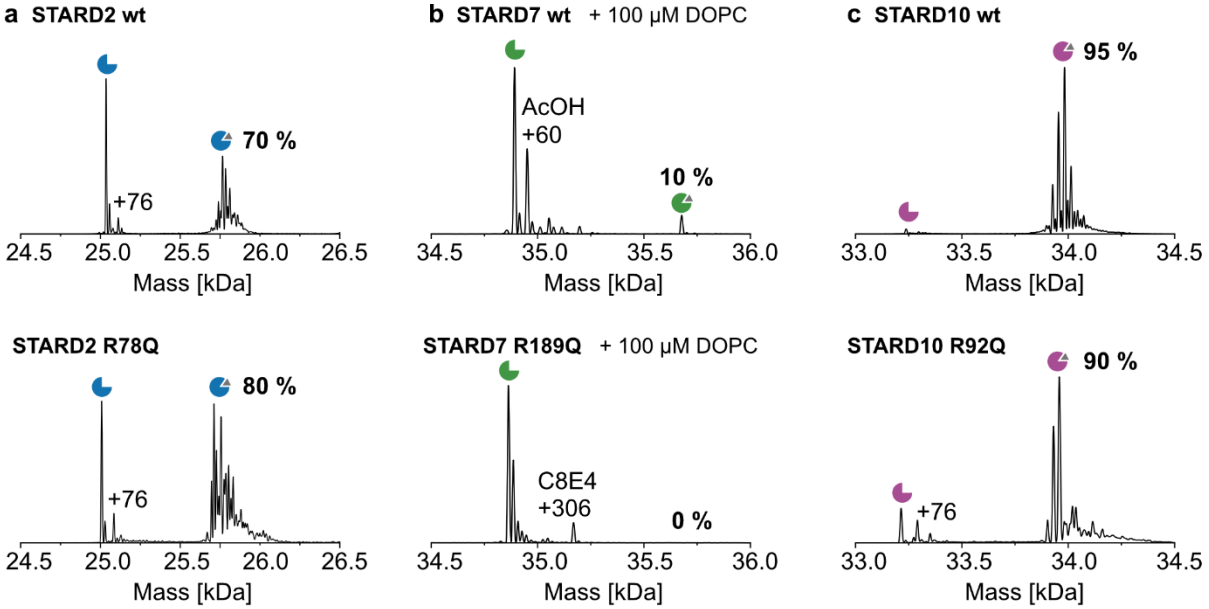

Figure S4. Lipid binding to STARD2 R78Q, STARD7(76–370) R189Q and STARD10 R92Q arginine-to-glutamine mutants. The point mutation does not reduce the ratio of phospholipids copurifying with STARD2 (**a**) and STARD10 (**c**) but abolishes lipid binding to STARD7(76–370) (**b**). The STARD7(76–370) R189Q mutant neither binds acetate nor phospholipids, when incubated with 100 µM DOPC in ammonium acetate + 2×CMC C8E4. Percentages are rounded to ±5 %.

Characterization of StARD proteins expressed in human cell lines

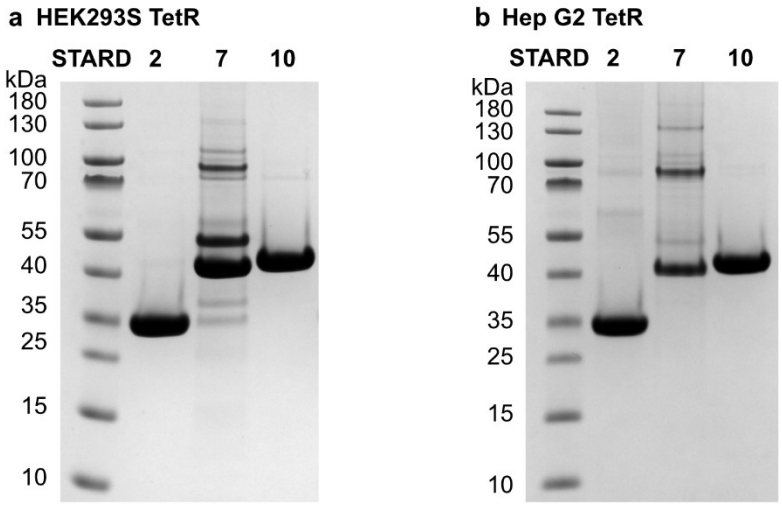

Figure S5. SDS-PAGE of STARD2, STARD7 and STARD10 expressed in HEK293S TetR cells (**a**) and HepG2 TetR cells (**b**) after elution from anti-FLAG beads.

Table S2. Characterization and quantification of phospholipids copurified with STARD2, STARD7 and STARD10 upon expression in HEK293S cells.

HEK293S

m/z (+)	Sum	Fatty acids	STARD2	STARD7	STARD10
704.52	PC 30:1	14:0_16:1			
730.54	PC 32:2	16:1_16:1			
732.55	PC 32:1	16:0_16:1			
758.57	PC 34:2	16:1_18:1			
760.59	PC 34:1	16:0_18:1			
786.60	PC 36:2	18:1_18:1			
788.62	PC 36:1	18:0_18:1			
814.63	PC 38:2	18:1_20:1			

m/z (−)	Sum	Fatty acids	STARD10
698.51	PE-P 34:2	16:1_18:1	
700.53	PE-P 34:1	16:0_18:1	
714.51	PE 34:2	16:1_18:1	
716.52	PE 34:1	16:0_18:1	
724.53	PE-P 36:3	18:1_18:2	
726.54	PE-P 36:2	18:1_18:1	
740.52	PE 36:3	18:1_18:2	
742.54	PE 36:2	18:1_18:1	
773.53	PG 36:2	18:1_18:1	

Table S3. Characterization and quantification of phospholipids copurified with STARD2, STARD7 and STARD10 upon expression in HepG2 cells.

HepG2

m/z (+)	Sum	Fatty acids	STARD2	STARD7	STARD10
730.54	PC 32:2	16:1_16:1			
732.55	PC 32:1	16:0_16:1			
756.55	PC 34:3	16:0_18:3 16:1_18:2			
758.57	PC 34:2	16:1_18:1 16:0_18:2			
760.59	PC 34:1	16:0_18:1			
780.55	PC 36:5	n.a.			
782.57	PC 36:4	n.a.			
784.59	PC 36:3	18:1_18:2			
786.60	PC 36:2	18:1_18:1			
788.62	PC 36:1	18:0_18:1			
804.55	PC 38:7	16:1_22:6			
806.57	PC 38:6	16:0_22:6			
808.59	PC 38:5	18:1_20:4			
810.60	PC 38:4	18:1_20:3			
832.59	PC 40:7	18:1_22:6			

Table S3 (continued).

m/z (−)	Sum	Fatty acids	STARD10
714.51	PE 34:2	16:1_18:1	
738.51	PE 36:4	18:1_18:3 16:0_20:4 16:1_20:3	
740.52	PE 36:3	18:1_18:2	
742.54	PE 36:2	18:1_18:1	
760.49	PE 38:7	16:1_22:6	
762.51	PE 38:6	16:0_22:6 18:1_20:5	
764.52	PE 38:5	18:1_20:4	
766.54	PE 38:4	18:1_20:3 18:0_20:4	
788.52	PE 40:7	18:1_22:6	
745.50	PG 34:2	16:1_18:1	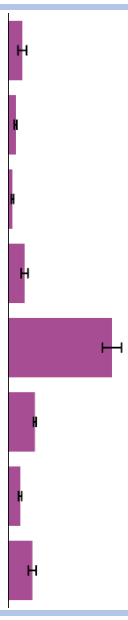
747.52	PG 34:1	16:0_18:1 16:1_18:0	
769.50	PG 36:4	16:1_20:3 18:2_18:2	
771.52	PG 36:3	18:1_18:2	
773.53	PG 36:2	18:1_18:1	
797.53	PG 38:4	18:1_20:3	
799.55	PG 38:3	18:1_20:2 18:0_20:3	
819.52	PG 40:7	18:1_22:6	

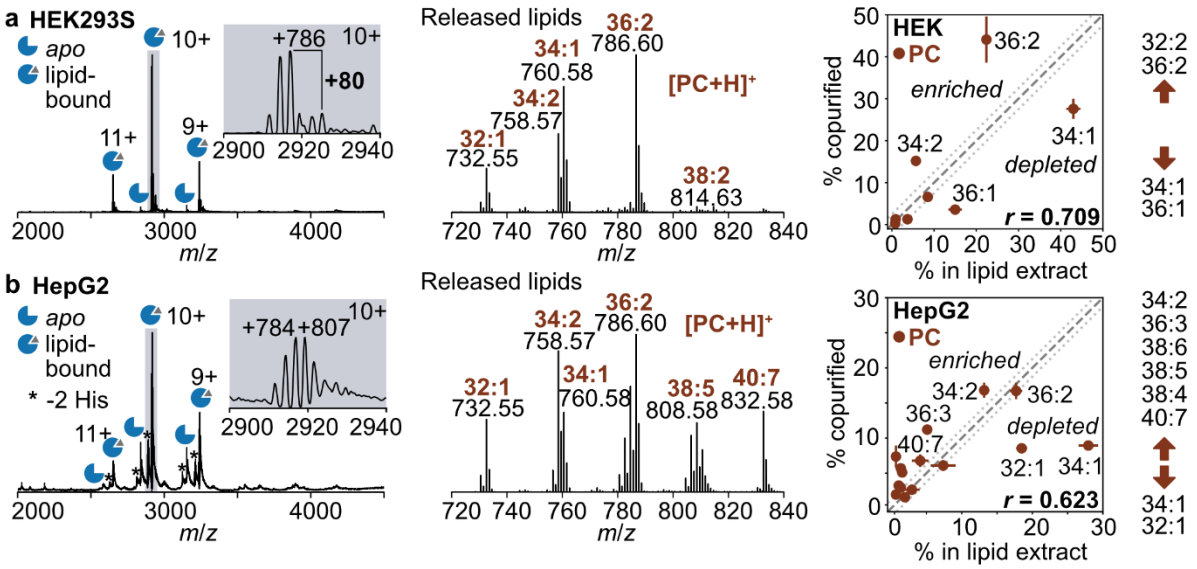

Figure S6. Ligands of STARD2 expressed in HEK293S (**a**) and HepG2 (**b**) cell lines. Monounsaturated PC lipids are consistently depleted across both cell lines.

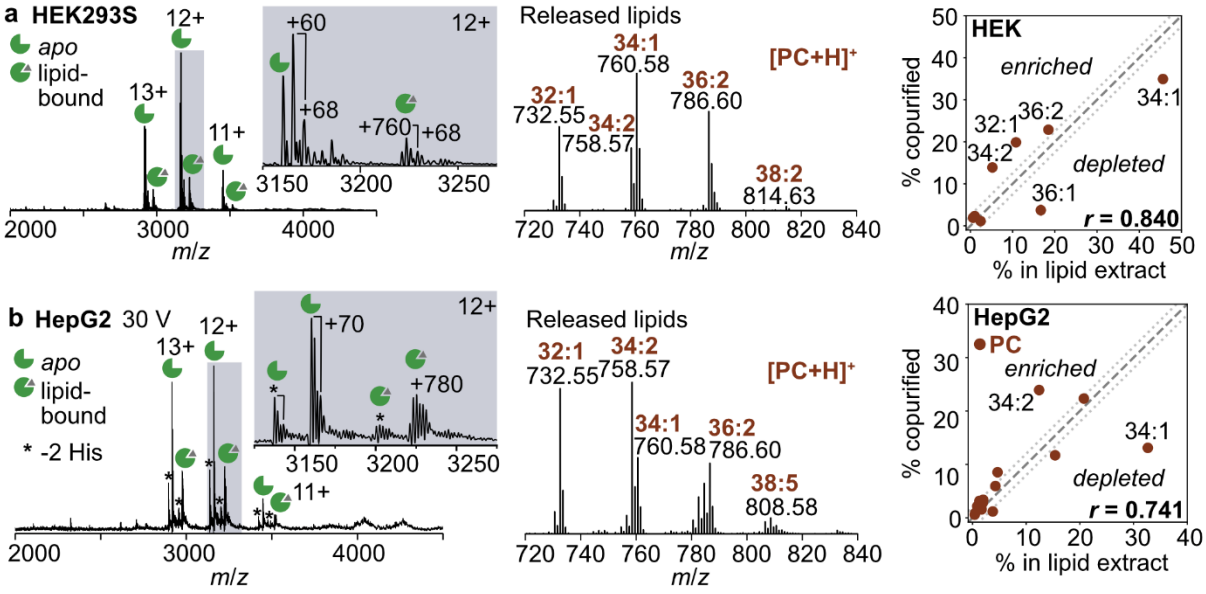

Figure S7. Ligands of STARD7 expressed in HEK293S (**a**) and HepG2 (**b**) cell lines. Phosphatidylcholines released from purified STARD7 show a high correlation with the cellular lipid composition, suggesting little acyl chain selectivity.

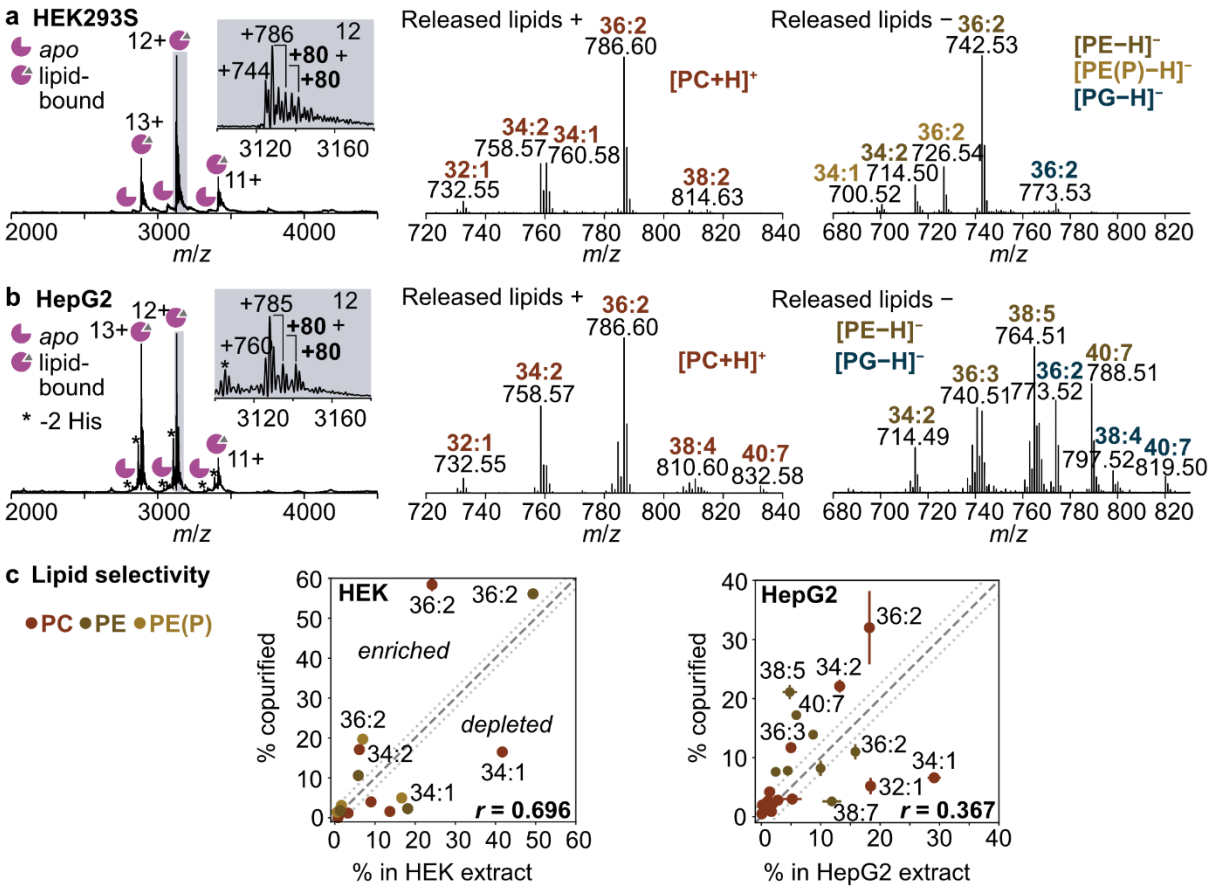

Figure S8. Ligands of STARD10 expressed in HEK293S (**a**) and HepG2 (**b**) cell lines. Phospholipids were released in positive and negative ion modes to detect different lipid classes. **c.** STARD10 copurifies with phospholipids with a high acyl chain selectivity, causing weak correlations between the copurified lipids and respective lipid extracts.

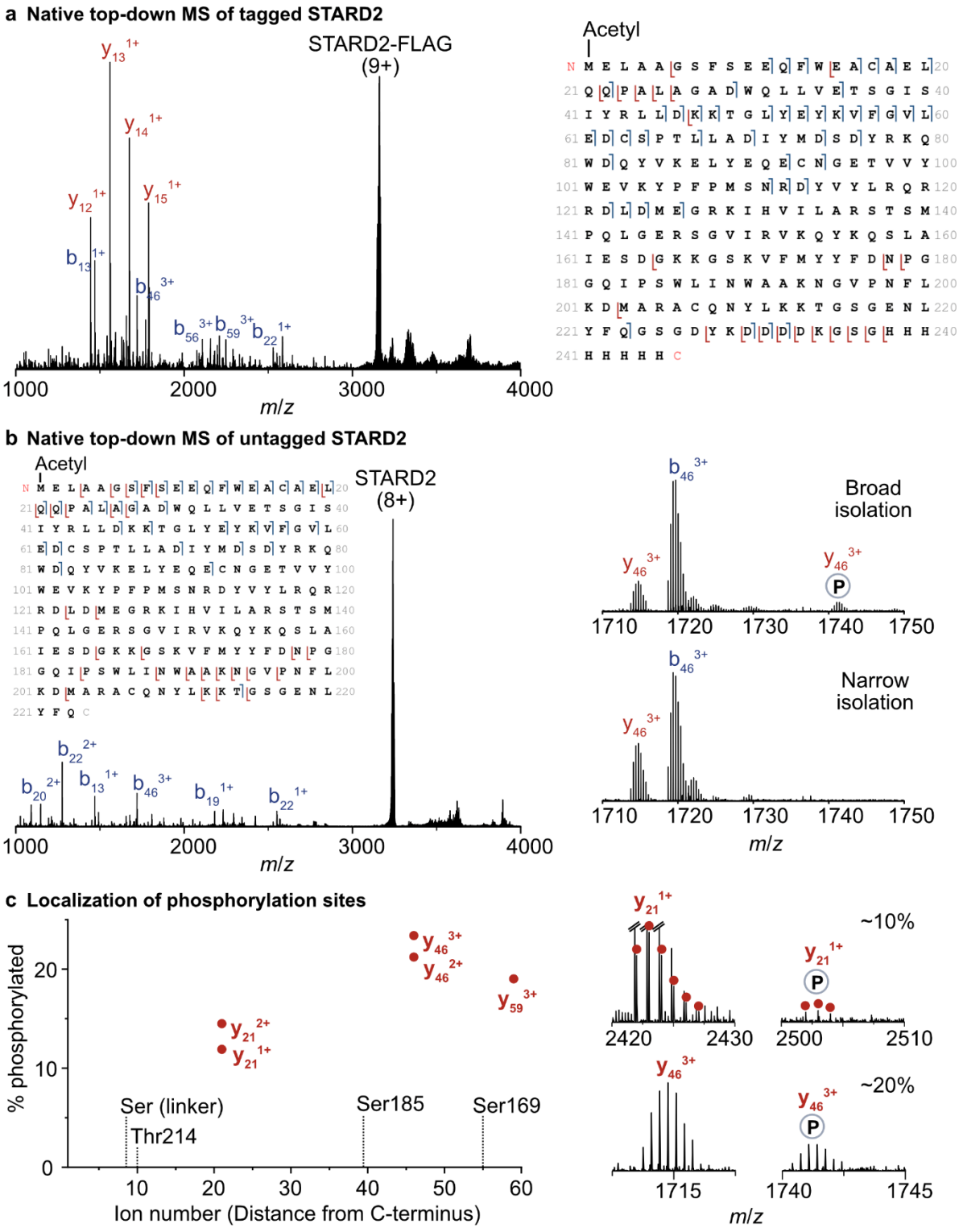

Figure S9. Native top-down MS of STARD2. **a.** Fragmentation of FLAG-tagged STARD2 (9+ charge state, HCD 80V) did not yield phosphorylated peptides. **b.** After cleavage of the FLAG tag, C-terminal fragments with hosphate modification were obtained (8+ charge state, HCD 70 V). Phosphorylated fragments were observed when the phosphorylated precursor ion was included in the isolation window (*m*/*z* 3245 ± 10), and were absent when the *apo* protein was isolated alone (*m*/*z* 3240 ± 5). **c.** Two phosphorylation sites with ca. 10 % occupancy each were detected: Thr214 or Ser in the GSG linker (exact position cannot be determined), and Ser185. Relative intensities of phosphorylated fragments are exemplarily shown for y21 and y46 ions. All b-type ions carry an acetyl modification, supporting N-acetylation of the protein.

STARD2

MELAAGSFSEEQFWEACAELQQPALAGADWQLLVETSGISIYRLLDKKTGLYEYKVFGVLEDCSPTLLADIYMDSDYRKQWDQY

VKELYEQECNGETVVYWEVKYPFPMSNRDYVYLRQRRDLDMEGRKIHVILARSTSMPQLGERSGVIRVKQYKQSLAIESDGKKG

SKVFMYYFDNPGGQIPSWLINWAAKNGVPNFLKDMARACQNYLKKTGSGENLYFQGSGDYKDDDDKGSGHHHHHHHH

171 185 137 213

Linker TEV protease cleavage site FLAG tag His8 tag

Figure S10. Proteomics analysis of STARD2 after in-gel digestion. The sequence map shows detected phosphorylated peptides (underlined). All peptides are 2–3 % phosphorylated. Ser185 is highlighted.

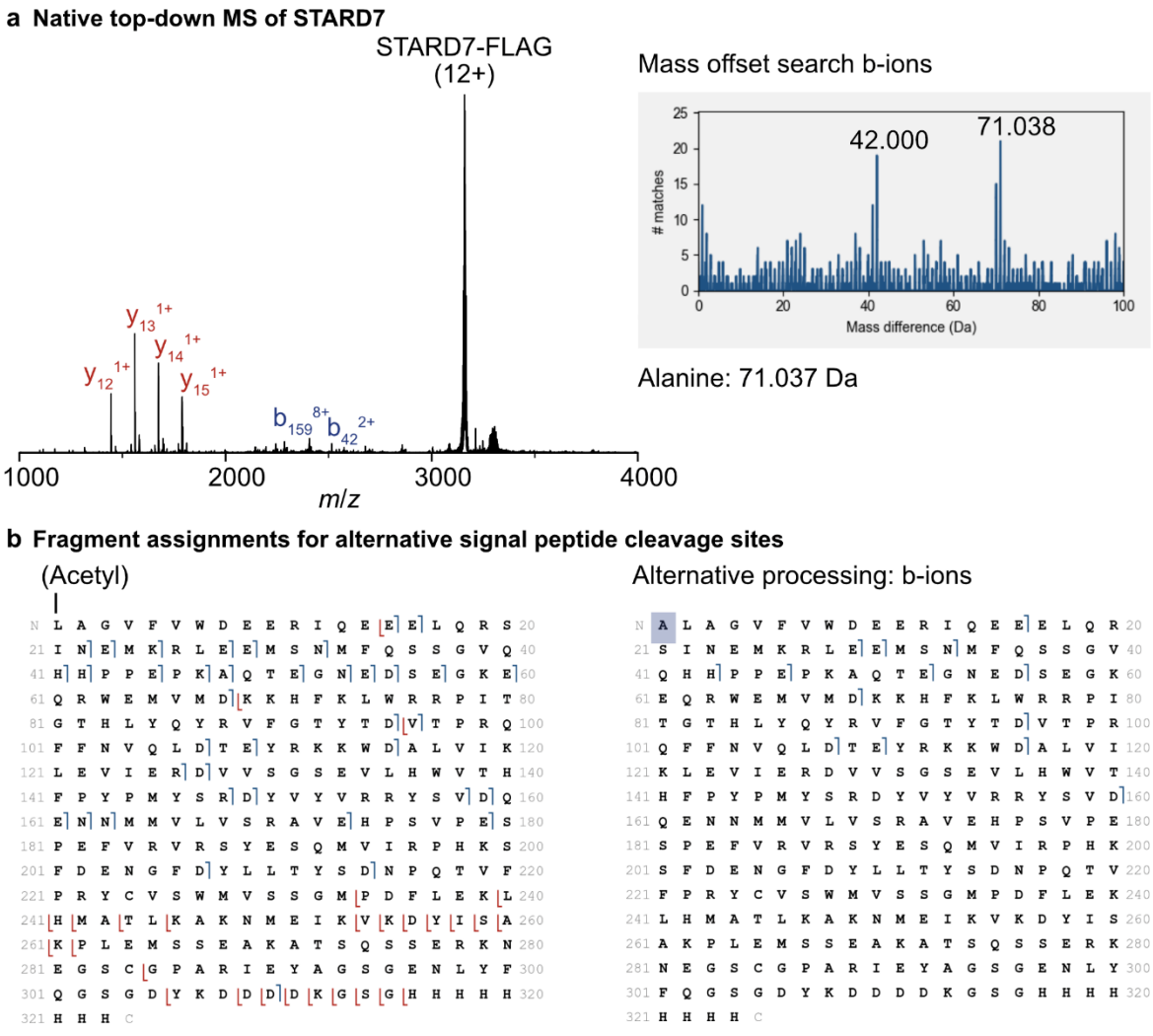

Figure S11. Native top-down MS of STARD7 (12+ charge state, HCD 100V). **a.** The majority of sequence ions can be assigned to STARD7 cleaved between A78 and L79. A mass offset search of unassigned fragment ions showed that another set of fragment ions is shifted by the mass of an additional alanine (Δm = 71 Da), suggesting alternative cleavage between A77 and A78. **b.** Fragment maps for both protein isoforms are shown (blue: b-type ions, red: y-type ions). Because y-type ions are identical for both isoforms, only b-type ions revealing the alternative cleavage site are shown for the minor isoform.

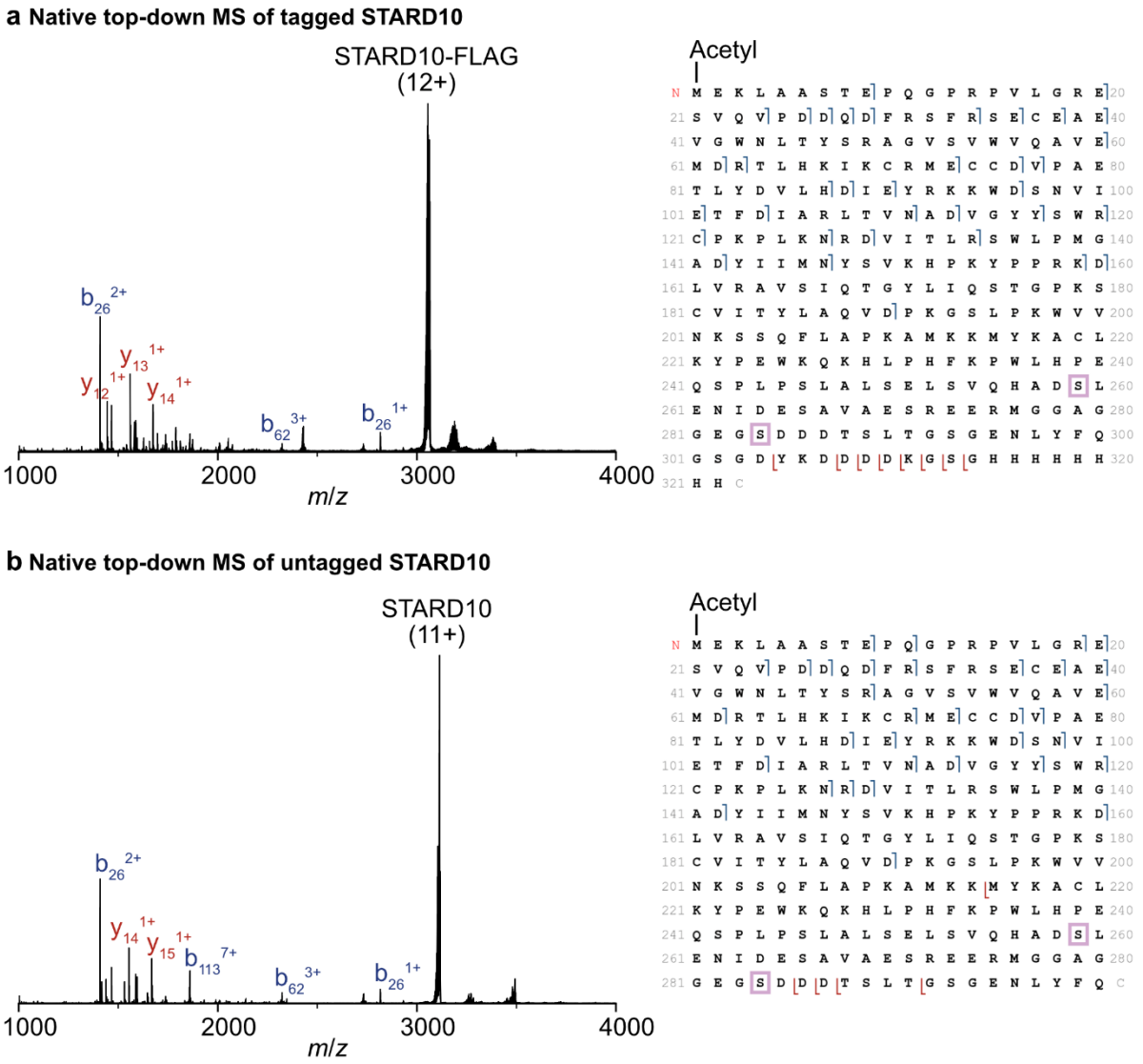

Figure S12. Native top-down MS of STARD10. Fragmentation of **a.** FLAG-tagged STARD10 (12+ charge state, HCD 80V) and **b.** untagged STARD10 (11+ charge state, HCD 70 V) did not yield phosphorylated fragments. Fragments were not generated in the region containing the two main phosphorylation sites (S259 and S284; pink). Detected cleavage sites are indicated in the sequence map (blue: b-type ions, red: y-type ions). All detected b-type ions carry an acetyl modification, supporting complete N-acetylation of the protein.

STARD10

MEKLAASTEPQGPRPVLGRESVQVPDDQDFRSFRSECEAEVGWNLTYSRAGVSVWVQAVEMDRTLHKIKCRMECCDVPAETL

YDVLHDIEYRKKWDSNVIETFDIARLTVNADVGYYSWRCPKPLKNRDVITLRSWLPMGADYIIMNYSVKHPKYPPRKDLVRAVSI

QTGYLIQSTGPKSCVITYLAQVDPKGSLPKWVVNKSSQFLAPKAMKKMYKACLKYPEWKQK(229)HLPHFKPWLHPEQSPLPSLALSE

LSVQHAD(259)**S**LENIDESAVAESREER(276)MGGAGGEG(284)**S**DDDTSLTGSGENLYFQGSGDYKDDDDKGSGHHHHHHHH

Linker **TEV protease cleavage site** **FLAG tag** **His8 tag**

Figure S13. Proteomics analysis of STARD10. The sequence map shows two detected peptides with phosphate modifications (underlined). Both peptides were 90–95 % phosphorylated. The main phosphorylation sites are highlighted (Ser259 and Ser284).

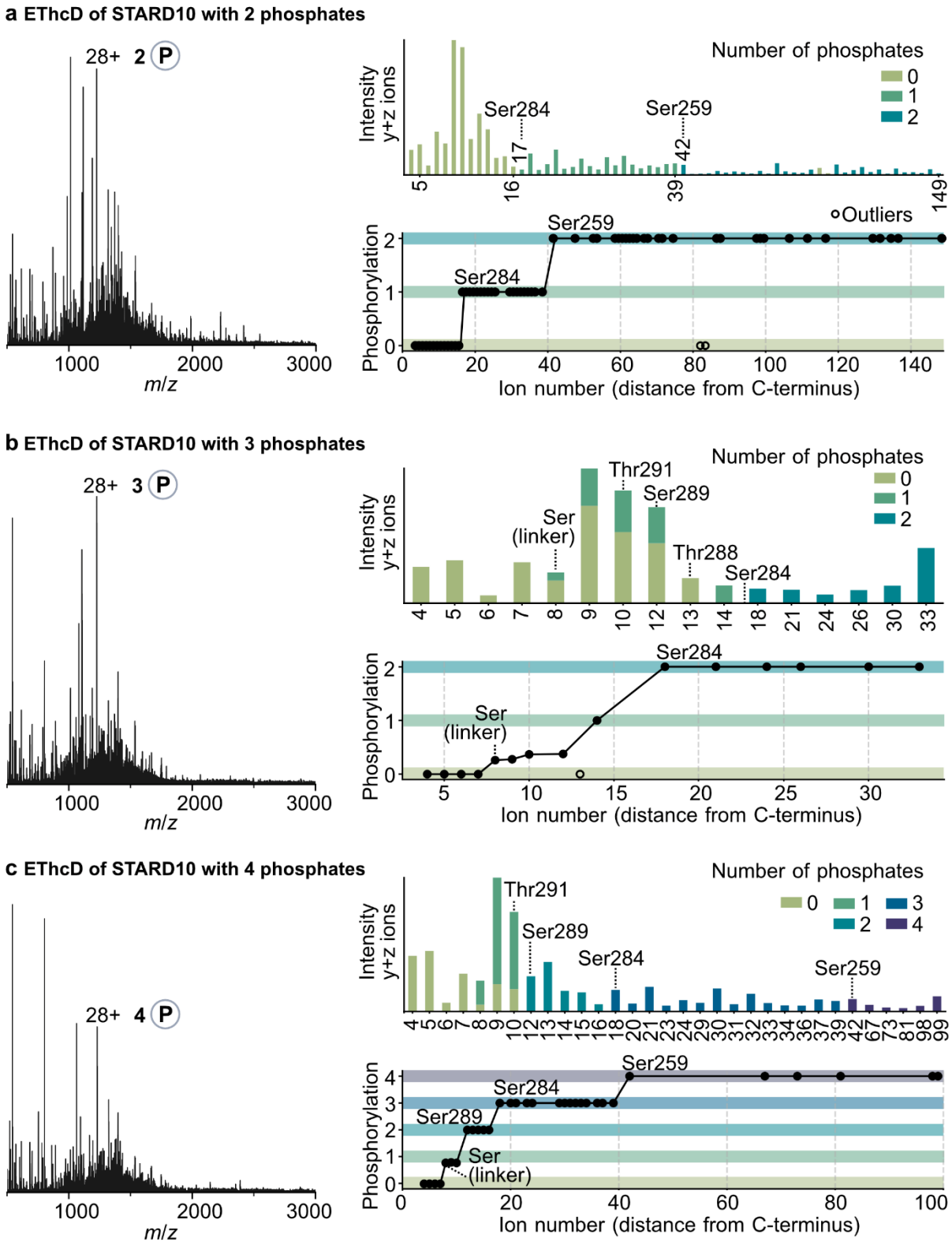

Figure S14. Denaturing top-down MS of STARD10 enables mapping of phosphorylation sites. STARD10 (28+ charge state) carrying two (*m*/*z* 1224 ± 1), three (*m*/*z* 1228 ± 1) or four (*m*/*z* 1230 ± 1) phosphates was fragmented by EThcD (1.5 ms, 30 % NCE). By comparing the number of phosphates on y- and z-ions of different length, phosphorylation sites were mapped. Ser284 and Ser259 are constitutively phosphorylated. Additional, partially occupied phosphorylation sites include the serine in the linker (GSG) and three C-terminal residues (Thr288, Ser289, Thr291).

Correlations between protein expression and lipid metabolism

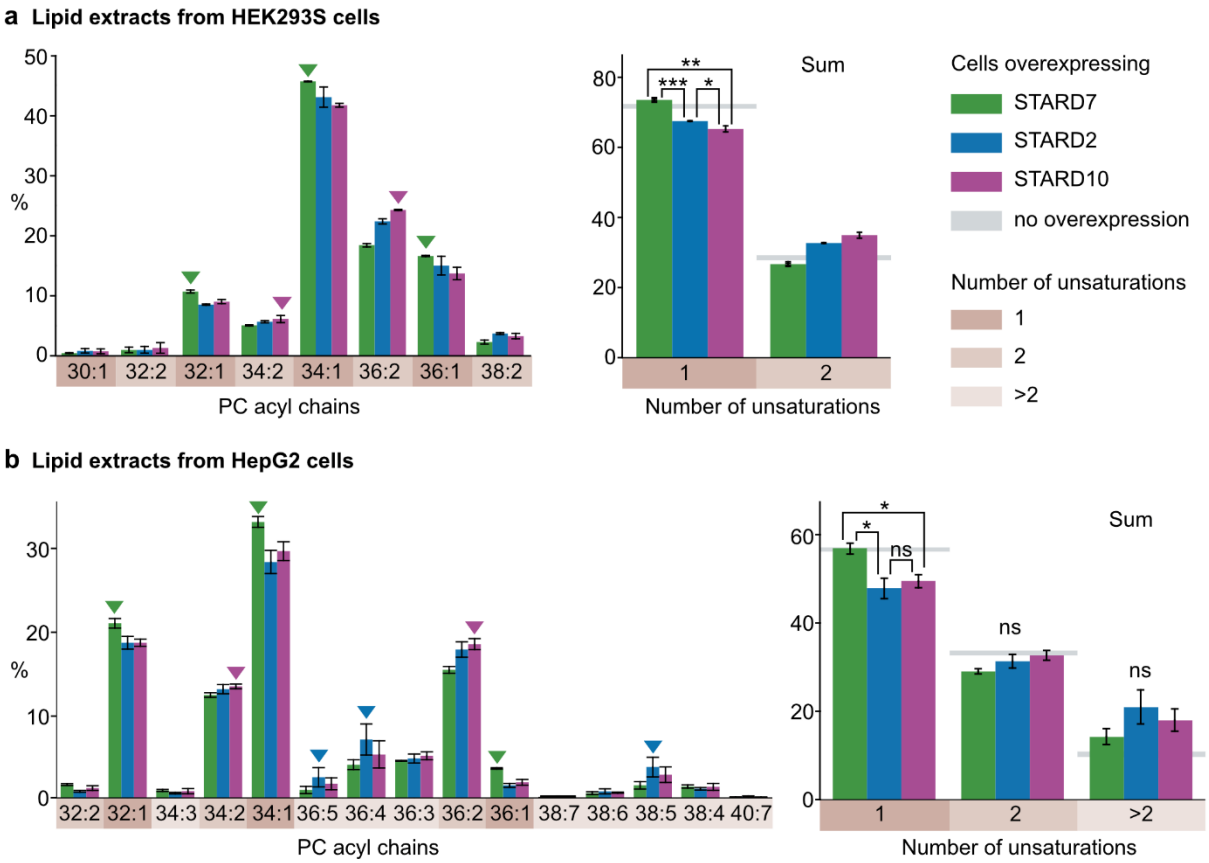

Figure S15. Overexpression of STARD2, STARD7 or STARD10 in HEK293S and HepG2 cell lines consistently changes cellular lipid profiles. **a.** Lipid extraction from HEK293S cells overexpressing STARD2, STARD7 or STARD10 shows that LTPs shift cellular PC ratios according to their acyl chain selectivities **b.** Lipid extraction from HepG2 cells overexpressing STARD2, STARD7 or STARD10 confirms a reduced ratio of monounsaturated PC upon overexpression of STARD2 and STARD10.

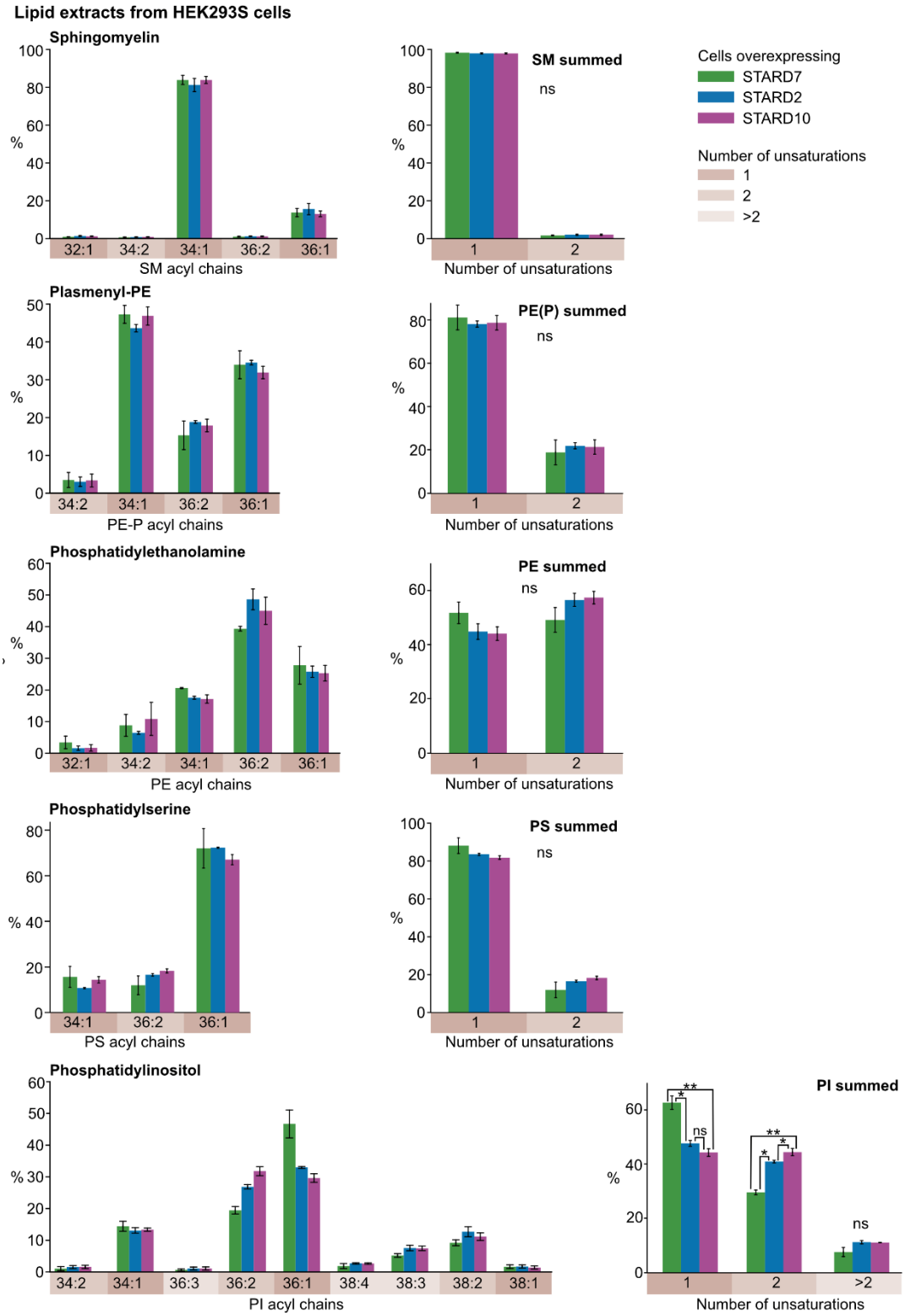

Figure S16. Acyl chain profiles of different phospholipid classes in HEK293S cells overexpressing STARD2, STARD7 or STARD10. PE species follow a similar trend as PC but show no statistical significance. The acyl chain profiles of PI are significantly affected by overexpression of the LTPs (significance shown based on q-values).

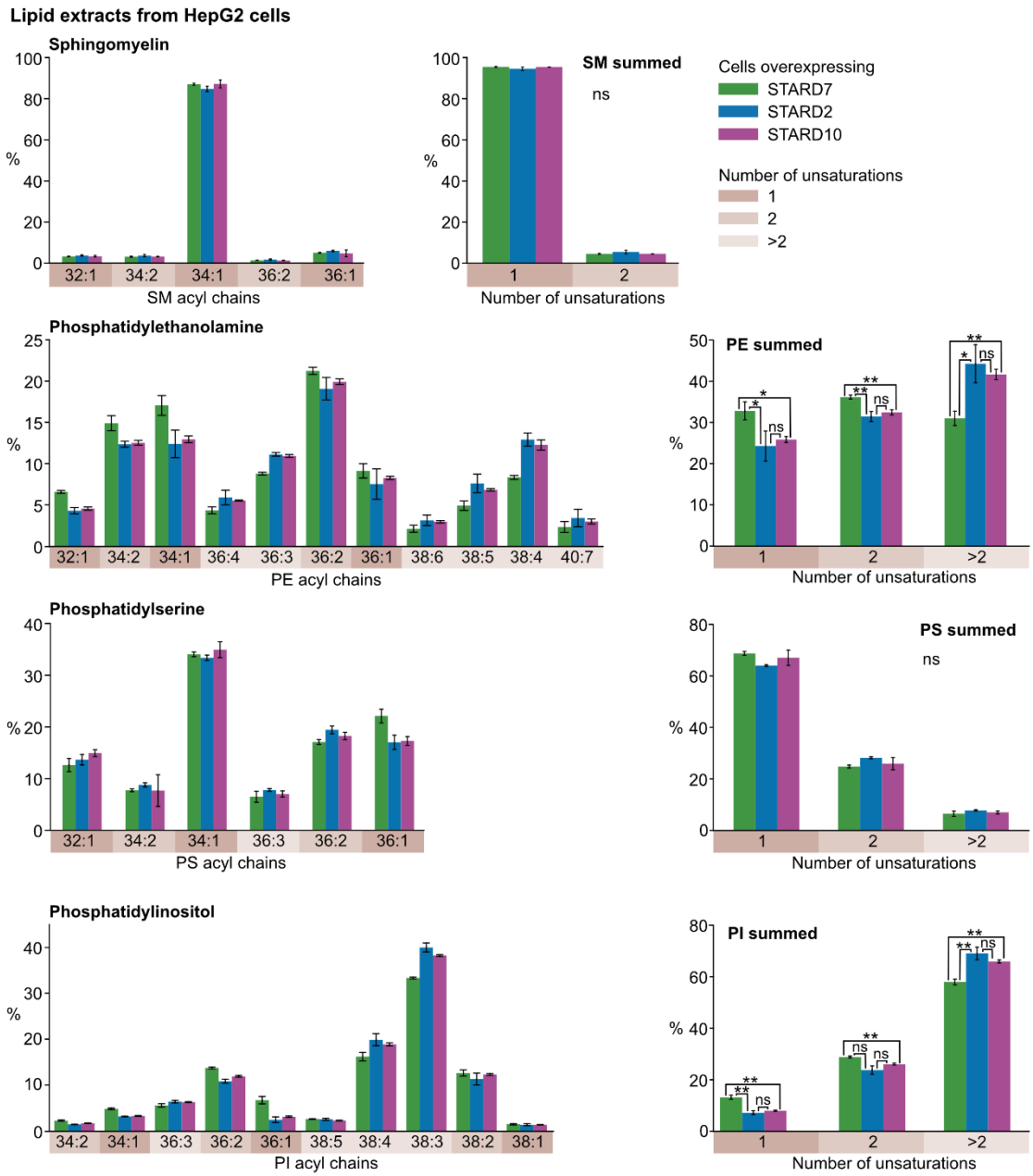

Figure S17. Acyl chain profiles of different phospholipid classes in HepG2 cells overexpressing STARD2, STARD7 or STARD10. PE and PI acyl chains change following a similar trend as PC (significance shown based on q-values).

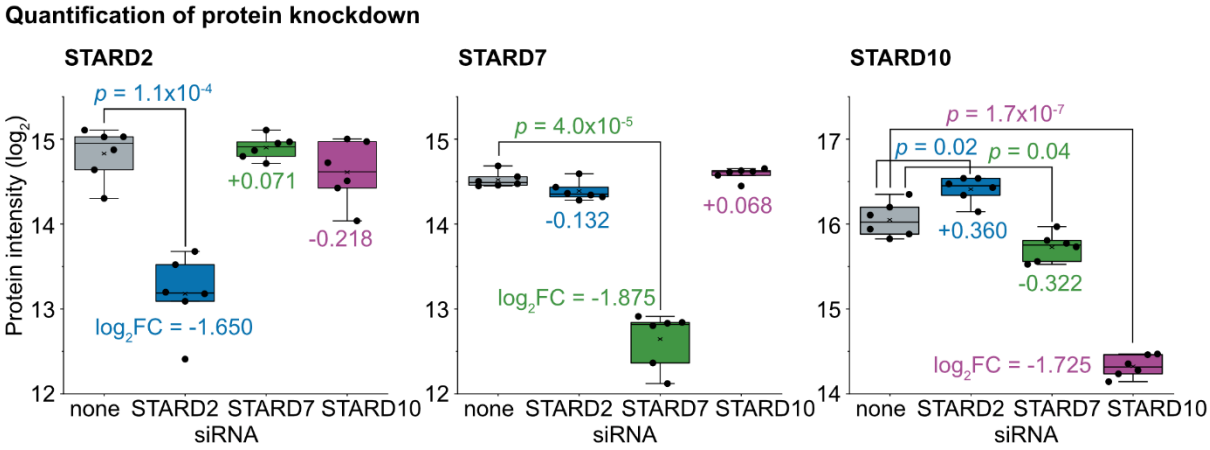

Figure S18. Changes in the cellular proteome upon siRNA-mediated knockdown of STARD2, STARD7 or STARD10 quantified by MS-based proteomics. p-values were obtained from pairwise Welch's t-tests comparing the control to each of the three siRNA knockdown conditions, with Bonferroni correction applied for multiple testing. Only statistically significant p-values are shown. Log_2-fold changes are reported for all conditions relative to the control sample.

Table S4. Precursor isolation windows for dia-PASEF.

Scan Type	Ramp	Mass Start [Da]	Mass End [Da]	Ion mobility Start [Vs/cm^2]	Ion mobility End [Vs/cm^2]
MS^1	0				
dia-PASEF	1	400	425	0.64	0.83
dia-PASEF	1	600	625	0.83	1.01
dia-PASEF	1	800	825	1.01	1.37
dia-PASEF	2	425	450	0.64	0.85
dia-PASEF	2	625	650	0.85	1.04
dia-PASEF	2	825	850	1.04	1.37
dia-PASEF	3	450	475	0.64	0.87
dia-PASEF	3	650	675	0.87	1.06
dia-PASEF	3	850	875	1.06	1.37
dia-PASEF	4	475	500	0.64	0.90
dia-PASEF	4	675	700	0.90	1.09
dia-PASEF	4	875	900	1.09	1.37
dia-PASEF	5	500	525	0.64	0.92
dia-PASEF	5	700	725	0.92	1.11
dia-PASEF	5	900	925	1.11	1.37
dia-PASEF	6	525	550	0.64	0.94
dia-PASEF	6	725	750	0.94	1.13
dia-PASEF	6	925	950	1.13	1.37
dia-PASEF	7	550	575	0.64	0.97
dia-PASEF	7	750	775	0.97	1.16
dia-PASEF	7	950	975	1.16	1.37
dia-PASEF	8	575	600	0.64	0.99
dia-PASEF	8	775	800	0.99	1.18
dia-PASEF	8	975	1000	1.18	1.37

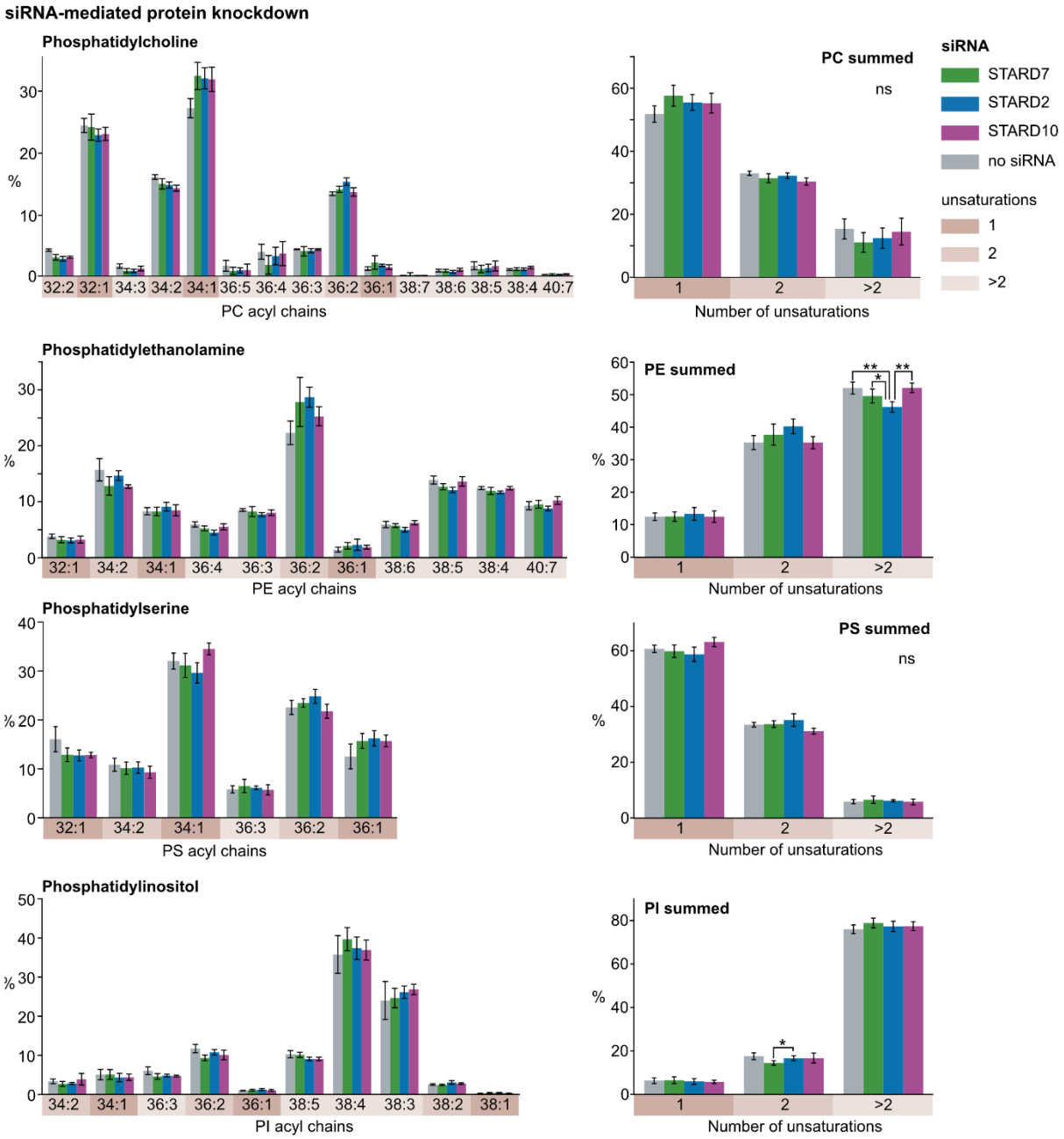

Figure S19. Acyl chain profiles of different phospholipid classes in HepG2 cells following 72 h siRNA-mediated knockdown of STARD2, STARD7 or STARD10. Polyunsaturated PE is reduced in STARD2 knockdown cells. Statistical significance is shown based on q-values.

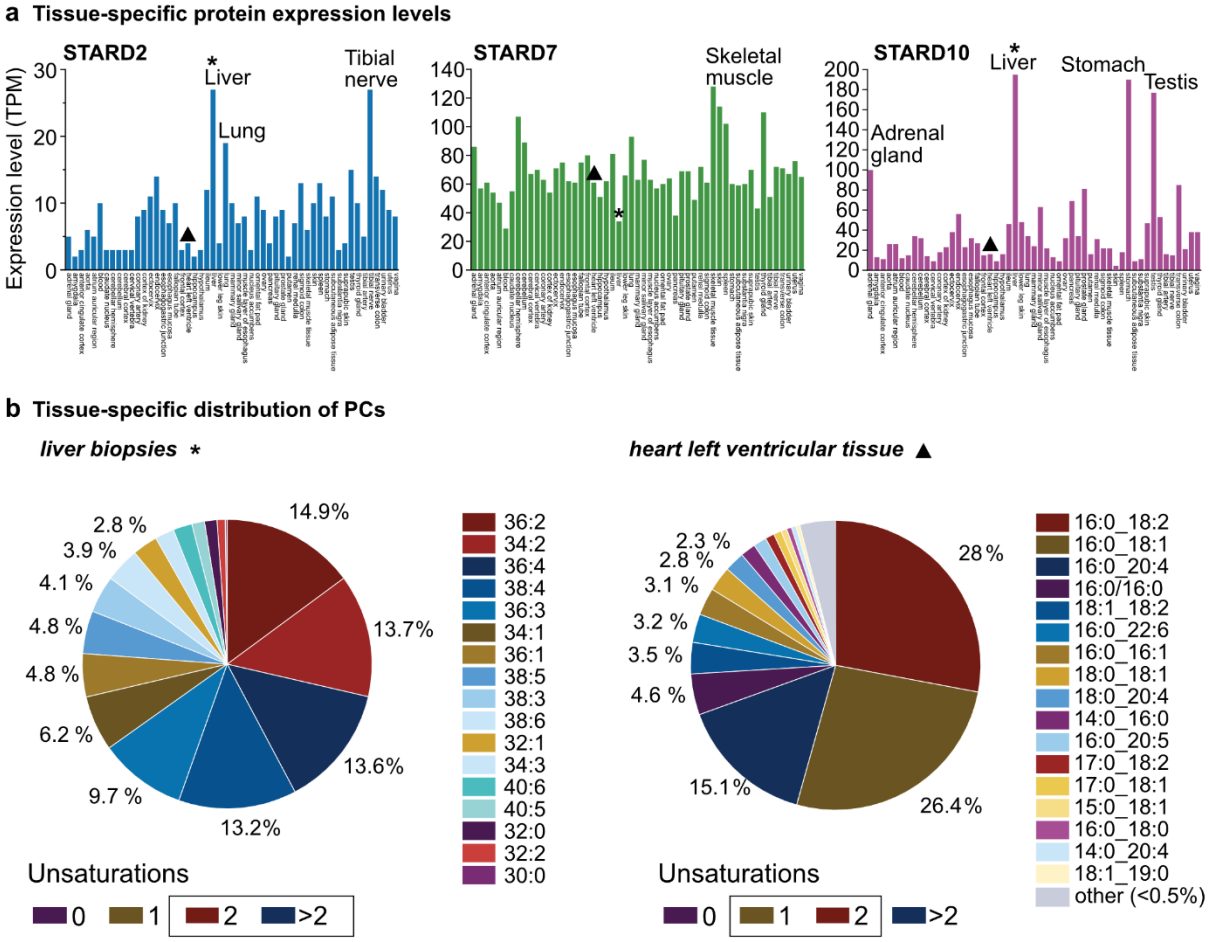

Figure S20. Correlation between expression levels of STARD phospholipid transfer proteins and phosphatidylcholines in different tissues. **a.** Expression levels of STARD2, STARD7, and STARD10 in different human tissues (TPM = transcripts per million). Data were exported from the EMBL-EBI Expression Atlas (http://www.ebi.ac.uk/gxa).[1] **b.** Variation of the PC acyl chain composition in different tissues. Lipidomics analyses of human liver[2] and heart left ventricular tissue[3] are exemplarily shown. The liver samples mainly contain doubly and polyunsaturated PC lipids that are preferred ligands of STARD10 and STARD2, respectively. Though individual acyl chains were not detected, we infer from lipidomics data on HepG2 cells that doubly unsaturated PC 36:2 and 34:2 carry one unsaturation in each chain. Heart tissue contains a larger fraction of monounsaturated PC, and the preferred ligands of STARD10 are not detected.

In vitro lipid transfer assays

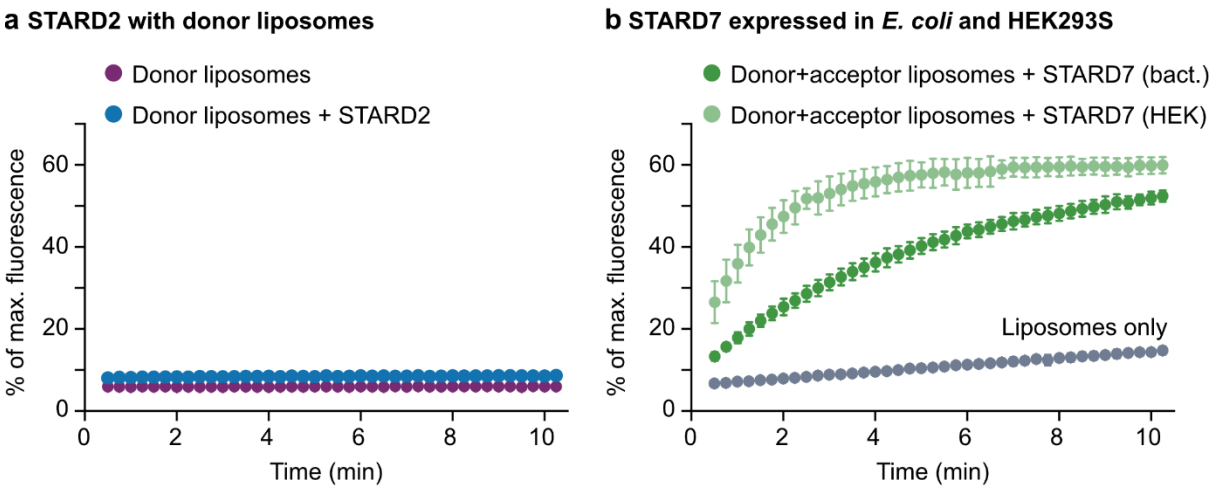

Figure S21. Control experiments for fluorescent lipid transfer assays. **a.** The addition of STARD2 to donor liposomes in the absence of acceptor liposomes yields constant fluorescence. **b.** STARD7 purified from HEK cells showed higher activity than STARD7 purified from bacteria.

Molecular dynamics simulations

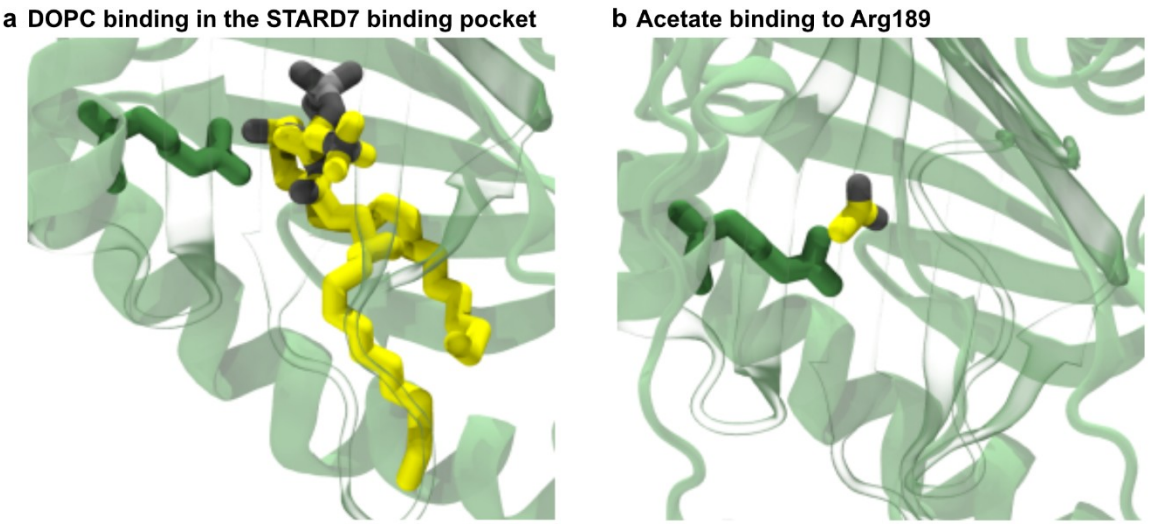

Figure S22. Boltz-2 prediction of the STARD7-acetate complex shows acetate binding to the conserved Arg189. **a.** Prediction of DOPC in the STARD7 lipid binding pocket. **b.** Prediction of acetate interacting with STARD7.

References

1 Kapushesky, M. *et al.* Gene expression atlas at the European bioinformatics institute. *Nucleic Acids Res.* **38**, D690–698 (2010).

2 Fahy, E. Biomarkers of NAFLD progression: a lipidomics approach to an epidemic. Part 1: Liver (2018). Metabolomics Workbench. Study ID: ST000915. Project DOI: https://doi.org/10.21228/M8V961

3 Koay, Y. C. Metabolomics studies on human cardiac samples (2023). Metabolomics Workbench. Study ID: ST003104. Project DOI: https://doi.org/10.21228/M8N42X